基于条件生成对抗网络的配准多模态脑MRI合成Synthesis of Registered Multimodal MRI with Lesion Label

Yili Qu,Wanqi Su,Chufu Deng,
Ying Wang,Yutong Lu,Nong Xiao,Zhiguang Chen

School of Data and Computer Science

Sun Yet-Sen University

quyli@mail2.sysu.edu.cn

Abstract

在基于大量数据驱动的医学影像智能处理任务中，医学影像数据的收集和采集是非常困难的，尤其是配准的多模态医学影像数据。合成的医学影像数据可以很好地缓解数据不足的问题。我们基于无监督的条件生成对抗网络模型实现了完全从随机噪声生成配准的多模态医学影像，并且可以根据自由选定的病灶标签有效地生成对应的病灶信息。我们在BRATS2015上进行了多项验证实验，验证了我们的合成MRI可以在医学影像智能处理任务中作为预训练数据或增强数据使用，并能大幅度提高模型的泛化能力。 In a large number of data-driven medical image intelligent processing tasks, the collection and acquisition of medical image data is very difficult, especially the registered multimodal medical image data. Synthetic medical image data can well alleviate the problem of insufficient data. In this paper, based on the unsupervised CGAN model, we achieve the generation of registered multimodal medical images from random noise and corresponding lesion information can be efficiently generated based on the freely selected lesion label. We conducted a number of validation experiments on BRATS2015 to verify that our synthetic MRI can be used as pre-trained data or enhanced data in medical image intelligent processing tasks, and can greatly improve the generalization ability of the model.

1 Introduction

核磁共振成像（MRI）是一种常见的医学影像，根据成像参数的不同可以有多种模态，例如T1、T2、T1c等。不同的模态对医生具有不同的参考价值，医生往往需要多个模态的影像互相对照才能做出准确的判断。在医学影像的智能处理任务的训练和学习中，我们往往也期望获得更多模态的影像，例如采用卷积神经网络（CNN）(Krizhevsky, Sutskever, and Hinton 2012)或生成对抗网络（GAN）(Goodfellow et al. 2014)进行的医学图像处理任务。 Magnetic resonance imaging (MRI) is a common medical image that can have multiple modalities depending on imaging parameters, such as T1, T2, T1c and so on. Different modalities have different reference values for doctors. To make accurate judgments, doctors often need multiple modal images to compare with each other. In the training and learning of medical image intelligent processing tasks, we often expect to obtain more modal images, such as medical image processing tasks based on Convolutional Neural Networks (CNN)(Krizhevsky, Sutskever, and Hinton 2012) or Generative Adversarial Networks (GAN)(Goodfellow et al. 2014).

当同一个病人的同一个部位通过不同的成像技术得到不同的模态时，如果成像位置和视角是一致的，那么得到的不同模态的影像就是对齐的，我们称之为这些模态之间是配准的。相较于单模态数据，配准的多模态影像数据能提供更多的信息，可以支撑更多和更复杂的应用场景，满足深度神经网络对训练数据的需求，有助于提供更加高效可靠的智能诊断服务。对于医生来说，获取不同模态的影像需要花费更长的时间并且需要患者的耐心配合。对于医学影像智能处理任务的研究者来说，多

模态的MRI数据集十分稀缺，收集难度非常大，尤其是罕见病数据，而配准的数据则更加稀少，这使得很多的训练任务无法实现。因此，通过应用图像合成技术扩展数据集，从已有的单模态图像转换为配准的多模态图像、从随机噪声生成配准的多模态医学影像，有着广泛的用途和深远的意义。 When obtaining different modalities from the same part of the same patient through different imaging techniques, these modalities are considered to be registered if the imaging position and the viewing angle are identical. Compared with unimodal data, the registered multimodal image data can provide more information, can support more complex application scenarios, meet the training data requirements of deep neural networks, and help to provide intelligent diagnostic services more efficient and more reliable. For doctors, it takes longer to acquire images of different modalities and requires patient patience. For researchers of medical image intelligent processing tasks, multimodal MRI datasets are scarce, and the collection is very difficult, especially rare disease data, and the registered data is even rarer, which makes many training tasks impossible. Therefore, the application of image synthesis technology to extend datasets, translate existing unimodal images to registered multimodal images, generate registered multimodal images from random noise, has a wide range of uses and far-reaching significance.

在GAN之前，一些研究使用图字典映射(Burgos et al. 2015)、稀疏编码(Huang, Shao, and Frangi 2017),(Vemulapalli, Van Nguyen, and Zhou 2015)，CNN(Van Nguyen, Zhou, and Vemulapalli 2015)等探索了医学影像的跨模态转换。此后许多研究使用GAN能产生更高质量的转换结果(Zhao et al. 2018),(Liang et al. 2018),(Zhu et al. 2017),(Choi et al. 2018)。得益于GAN的强大能力，目前，采用GAN实现跨模态医学影像转换成为主流(Zhang, Yang, and Zheng 2018),(Nie et al. 2017),(Osokin et al. 2017),(Van Nguyen, Zhou, and Vemulapalli 2015),(Kamnitsas et al. 2017)。一般的转换基于成对的数据，最近也有研究从不成对的跨域数据中学习(Zhang, Yang,

and Zheng 2018)。最近的研究有将像素到像素的GAN应用于脑部MRI到CT图像的转换(Nie et al. 2017),(Kamnitsas et al. 2017)、视网膜血管注释到图像的转换(Costa et al. 2017)、基于CycleGAN(Zhu et al. 2017)的心脏MRI到CT图像的相互转换与分割(Nie et al. 2017)等。对于多模态的合成，(Chartsias et al. 2018)实现多输入多输出的MRI合成，但对输入的多模态数据要求配准。基于此，(Joyce, Chartsias, and Tsaftaris 2017)改进实现存在缺失或未配准的多输入合成模型，能够从其输入的任何子集执行MRI图像合成，但限制了输出为单一模态，且模型不可扩展。(Miao et al. 2018)针对医学图像配准进行了深入研究。(Shin et al. 2018)应用GAN合成脑肿瘤图像实现数据增强和数据匿名化，但需要额外训练解剖结构分割网络，且要求数据集带有病灶分割标签，模型泛化能力弱。(Costa et al. 2017)研究了基于变分自编码器(VAE)(Kingma and Welling 2014),(Rezende, Mohamed, and Wierstra 2014)的思想实现血管注释图的随机生成，进而合成彩色视网膜图像。在当前的这些医学影像合成的研究中，大多仅探索了两个不同模态之间的转换合成(Zhang, Yang, and Zheng 2018),(Nie et al. 2017),(Burgos et al. 2015),(Vemulapalli, Van Nguyen, and Zhou 2015),(Osokin et al. 2017),(Van Nguyen, Zhou, and Vemulapalli 2015),(Kamnitsas et al. 2017)，对多模态的研究还很稀少(Chartsias et al. 2018),(Joyce, Chartsias, and Tsaftaris 2017),(Shin et al. 2018)，而在医学影像处理领域之外，多域转换的发展最近已经有了进展(Zhao et al. 2018),(Liang et al. 2018),(Choi et al. 2018),(Isola et al. 2017)。

Some studies explored cross-modal medical images translation prior to GAN by using graph dictionary mapping(Burgos et al. 2015), sparse coding(Huang, Shao, and Frangi 2017),(Vemulapalli, Van Nguyen, and Zhou 2015), and CNN(Van Nguyen, Zhou, and Vemulapalli 2015). Since then, many studies used GAN to generate higher quality translation results(Zhao et al. 2018),(Liang et al. 2018),(Zhu et al. 2017),(Choi et al. 2018). Owe to the powerful capabilities of GAN, it has become the mainstream to achieve multimodal medical image

translation(Zhang, Yang, and Zheng 2018),(Nie et al. 2017),(Osokin et al. 2017),(Van Nguyen, Zhou, and Vemulapalli 2015),(Kamnitsas et al. 2017). The general translation is based on paired data, some studies have also learned from unpaired cross-modal data(Zhang, Yang, and Zheng 2018). Recent studies have realized brain MRI to CT image translation with pixel-to-pixel GAN(Nie et al. 2017),(Kamnitsas et al. 2017), retinal vascular annotation to image translation(Costa et al. 2017), CycleGAN-based(Zhu et al. 2017) cardiac MRI to CT image translation and segmentation(Nie et al. 2017). For multimodal synthesis, (Chartsias et al. 2018) implements MRI synthesis of multiple inputs multiple outputs, but requires registration for input multimodal data. Based on this, (Joyce, Chartsias, and Tsaftaris 2017) improves and implements a missing or unregistered multi-input synthesis model that can perform MRI image synthesis from any subset of its inputs, but limits the output to a single modality and the model is not scalable. (Miao et al. 2018) has conducted in-depth research on medical image registration. (Shin et al. 2018) applys GAN to synthesize brain tumor images for data enhancement and data anonymization, but additional training of anatomical segmentation networks is required, and the dataset is required to have lesion segmentation labels, so the model generalization ability is weak. (Costa et al. 2017) studies the random generation of vascular annotation maps based on the idea of Variational Auto-Encoder (VAE)(Kingma and Welling 2014; **?**), and then synthesizes color retinal images. In these current studies of medical image synthesis, most are two-modal translation(Zhang, Yang, and Zheng 2018),(Nie et al. 2017),(Burgos et al. 2015),(Vemulapalli, Van Nguyen, and Zhou 2015),(Osokin et al. 2017),(Van Nguyen, Zhou, and Vemulapalli 2015),(Kamnitsas et al. 2017), and the study of multimodal translation is very rare(Chartsias et al. 2018),(Joyce, Chartsias, and Tsaftaris 2017),(Shin et al. 2018). Outside the field of medical image processing, the development of many-to-many translation has recently made progress(Zhao et al. 2018),(Liang et al. 2018),(Choi et al. 2018),(Isola et al. 2017).

目前针对医学影像合成的研究存在模态数量难以扩展、需要配准训练数据、依赖于复杂的大型网络、无法添加或保留病灶、无法从随机矩阵开始生成、需要额外的训练数据等各项问题，且大多数研究对合成数据的评价依赖于经验医师的人工视觉效果评估，没有进行客观的量化检验。因此，我们设计了一种基于条件生成对抗网络(CGAN)(Mirza and Osindero 2014)的配准多模态MRI生成的方法，采用无监督学习方法，训练数据无需配准，输入随机正态分布矩阵进而生成一组有病灶标签的多模态配准MRI。我们在BRATS2015数据集上进行了带肿瘤分割标签的脑多模态MRI生成实验，并验证了我们的合成数据中病灶信息的有效程度和合成数据在肿瘤病灶分割实验中的可用程度。我们将开源我们的代码。总的来说，我们的工作主要体现在以下三个方面： At present, there are various problems in the research of medical image synthesis, such as the difficulty of expanding the number of modalities, the need to registered training data, relying on complex large networks, the inability to add or retain lesions, the inability to generate from random matrices, and the need of additional training data, etc. Moreover, the evaluation of synthetic data in most studies relies on the evaluation of artificial visual effects by experienced physicians, without objective quantitative evaluation. Therefore, we design a registered multimodal MRI generation scheme based on the Conditional Generative Adversarial Networks (CGAN)(Mirza and Osindero 2014). With unsupervised learning method, training data do not need to be registered. Our solution can receive a random normal distribution as input to generate a set of labeled multimodal registration MRI. We perform multimodal brain MRI generation experiments with tumor segmentation labels on BRATS2015, and verify the effectiveness of lesion information and the availability of synthetic data in tumor lesion segmentation experiments. See the open source code for details. Specifically, our contribution is

in the following three areas:

- 结构特征图的提取与随机生成Extraction and Random Generation of Structural Feature Maps 我们针对脑MRI提出了一种解剖结构特征的提取方法，无需额外的解剖结构分割标签或标签提取训练，可直接从任意模态的真实影像提取得到结构特征，用以辅助GAN学习生成更合理的合成影像。我们训练了一个结构特征图生成器实现了从多维正态分布生成结构特征图。我们的提取方法可以直接获取真实影像的解剖结构特征，在提升合成影像质量同时不带来额外参数、计算开销小，而随机生成方法可以无限地生成丰富多样的结构特征图。We propose an extraction method for anatomical features for medical images. Without additional anatomical segmentation labels or label extraction training, structural feature maps can be extracted directly from real images of arbitrary modalities ,and assist GAN to learn to generate more reasonable synthetic images. The extraction method can directly obtain the anatomical features of real images, and improve the quality of synthetic images without introducing additional parameters and computation overhead. We also train a structural feature map generator to generate structural feature maps from multidimensional normal distribution. The random generation method can generate rich and diverse structural feature maps indefinitely.

- 带标签多模态配准影像的合成Synthesis of Registered Multimodal MRI with Lesion Label 我们使用随机生成的结构特征图，融合随机的病灶标签，通过生成器合成配准的多模态MRI。我们探讨了多种病灶生成指导方法，并通过病灶生成指导方法实现了在多模态MRI的合成过程中根据输入病灶标签有效地生成对应的病灶信息。在训练时我们无需配准的数据，除病灶标签外无需额外的标签数据，而合成的数据是配准的，输入的随机病灶标签即为合成数据的病灶标签。我们的方法能够便捷快速地构建带标签的配准多模态MRI数据集。 We use randomly generated structural feature maps to fuse with random lesion labels and then synthesize the registered multimodal MRIs through the generator. We explore a variety of lesion generation guidance methods to achieve effective mapping of lesions based on input lesion labels during multimodal MRI synthesis. In training, no registration data is required, no additional label data is required except for the lesion label, the synthetic data is registered, and the random lesion label is the lesion label of the synthetic data. Our solution enables fast and easy construction of registered multimodal MRI datasets with label.

- 合成数据可用性的客观验证方法Objective Verification Method for Synthetic Data Availability 我们使用不同数据量的合成数据和真实数据构建的数据集来训练病灶分割网络，验证了合成数据可以在医学影像智能处理任务可以作为预训练数据和增强数据来提高模型的泛化能力从而提高分割精度。对比传统合成影像质量的主观评价方法，我们更加客观地呈现了合成数据在智能病灶处理任务中的可用性。 We construct datasets with different amount of synthetic and real data to train the lesion segmentor, and verify that the synthetic data can be used as pre-training data and enhanced data in the medical image intelligent processing tasks to improve the generalization ability of the model and improve the segmentation precision. Compared with the traditional subjective evaluation method of synthetic image quality, we present the availability of synthetic data in intelligent lesion processing tasks more objectively.

2 方法Method

我们在多模态脑MRI的合成任务上展示我们的方法。在本文的实例中，我们合成的病灶为肿瘤，病灶标签为肿瘤分割标签，病灶处理任务为病灶分割。我们的方法对合成部位、病灶类型、病灶处理任务、具体的模态和模态数量等不做限制，通过下述实例的展示，我们能很容易的将该方法推广应用到其他的类似任务。 We perform our scheme on multimodal brain MRI synthesis task, in which the synthetic lesion is tumors, the lesion label is a tumor segmentation
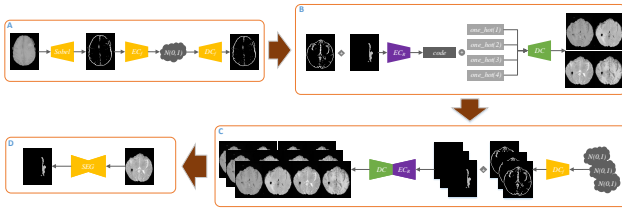
图 1: 整体架构图.Overall Architecture.

label, and the lesion processing task is lesion segmentation. Our scheme does not limit the synthesis of human parts, lesion types, lesion processing tasks, specific modality and the number of modalities. We can easily apply this method to other similar tasks through the following example.

2.1 整体架构Overall Architecture

如图 1所示，我们的方案包括结构特征图提取和生成、多模态MRI生成、构建合成数据集、合成数据可用性验证四个主要阶段。 As shown in Fig. 1, our scheme includes four main stages: structural feature map extraction and random generation, multimodal MRI generation, construction of synthetic datasets, and synthetic data availability verification.

结构特征图提取和生成阶段我们将获得一个结构特征图生成器，能从随机的正态分布矩阵生成结构特征图。该阶段我们训练的模型模包括一个结构特征图编码器、一个结构特征图解码器、一个结构特征图鉴别器、一个编码分布鉴别器和一个结构特征图掩膜生成器。 In the structural feature map extraction and random generation stage, we will obtain a structural feature map generator that can generate structural feature maps from the random normal distribution matrix. Models we train at this stage includes a structural feature map encoder, a structural feature map decoder, a structural feature map discriminator, a code distribution discriminator and a structural feature mask generator.

多模态MRI生成阶段我们产出一个条件生成器，其以结构特征图为输入，能根据不同的独热条件向量生成不同模态的MRI，并且可在结构特征图上添加病灶标签使得生成的MRI具有对应的病灶信

息。该阶段我们训练的模型模块包括一个结构特征图与病灶标签的融合图编码器、不同模态的病灶分割器、一个MRI编码器、一个MRI解码器、一个MRI鉴别器和一个MRI编码鉴别器。 In the multimodal MRI generation stage, we generate a conditional generator with input of structural feature maps, which can generate MRIs of different modalities according to different one-hot conditional vectors, and can add lesion labels on the structural feature maps to generate MRI has corresponding lesion information. At this stage, we train a structural feature map and lesion label fusion encoder, a lesion segmentor for each modality, an MRI encoder, an MRI decoder, an MRI discriminator and an MRI code discriminator.

在构建合成数据集阶段，我们使用前两个阶段产出的模型先从随机正态分布矩阵生成足量的结构特征图，再与随机病灶标签进行信息融合，最后通过条件生成器生成配准的多模态MRI，从而构建出一个合成数据集。 In the stage of constructing the synthetic datasets, we use the model produced in the first two stages to generate a sufficient number of structural feature maps from the random normal distribution matrix and then randomly fuse with real lesion labels, and finally generate the registered multimodal MRI to construct synthetic datasets.

在合成数据可用性验证阶段，我们首先根据真实的数据为每个MRI模态单独训练一个病灶分割器，并在真实数据集中进行分割能力测试，再用该分割器对采用不同的病灶生成组件来指导病灶生成的合成数据进行分割测试。然后，我们使用由不同数据量的合成数据和真实数据构建的数据集来对病灶分割网络进行训练，训练充分后再在真实测试数据集上进行分割测试，对比各项测试结果，以验证合成数据在肿瘤病灶分割训练中的可用性。 In the synthetic data availability verification stage, we train a lesion segmentor for each MRI modality based on real data, and perform segmentation ability tests on real dataset. Then these segmentors are used to perform segmentation tests on the synthetic data generated by different lesion gen-

eration guidance methods. In addition, we use datasets constructed from synthetic data and real data of different amounts to train the lesion segmentor. After training, the segmentation ability test is performed on the real dataset, and the test results are compared to verify the availability of the synthetic data in lesion segmentor training.

2.2 结构特征图提取方法Structural Feature Map Extraction Method

直接从随机噪声通过生成对抗训练生成的医学影像通常训练困难且难以生成真实的结构信息。我们将医学影像中提供基本轮廓和结构信息的图像称为其结构特征图，例如视网膜血管分布图可视为视网膜图像的结构特征图(Costa et al. 2017)。结构特征图可以为医学影像的合成提供必要的基础指导信息，例如合成脑部MRI图像时一些研究从脑分割标签图获取基本的结构信息(Shin et al. 2018)。然而，视网膜血管分布图和脑分割标签图等常用的结构特征图都需要额外的数据和训练才能实现从原图提取出结构特征图。为此，我们首先设计了下述直接从脑MRI提取结构特征图的方法，该方法具有运算快、无需训练、无需额外数据等优点。 Medical images generated directly from random noise by GAN are often difficult to train and difficult to generate real structural information. We call image that provide basic contour and structure information as structural feature map. For example, a retinal blood vessel distribution map can be regarded as a structural feature map of a retinal image(Costa et al. 2017). Structural feature maps can provide necessary basic guidance for the synthesis of medical images. For example, when synthesizing brain MRI, some studies obtain basic structural information from the brain segmentation label(Shin et al. 2018). However, common structural features such as retinal vascular maps and brain segmentation labels require additional data and training to extract structural features from the original image. To this end, we first design a method for extracting structural feature maps directly from brain MRI, which has the advantages of fast operation, no training, no additional data. 在传统的数字图像处理方法中，Roberts算子(G

1965)、Prewitt算子(Prewitt 1970)、Sobel算子(Sobel 1970)等是十分优秀的边缘检测算子，其中Sobel算子常用于脑部医学图像的处理，其卷积核参数和计算公式如图所示。我们探索出了从Sobel算子生成的边缘检测图中进一步提取结构特征的方法，如算法1所示。 In the traditional digital image processing methods, Roberts operator, Prewitt operator, Sobel operator, etc. are excellent edge detection operators. Sobel operator is often used in processing of brain medical images, and their convolution kernel parameters and calculation formula are as shown. As shown in Algorithm 1, We explore a method for further extracting structural feature maps from the edge detection maps generated by Sobel operator.

Algorithm 1 Structural Feature Extraction

1: Input a real image x,$beta$ is pixel threshold
2: $f1 = reduce\_min(sobel(x))$
3: $f2 = reduce\_max(sobel(x))$
4: $f1 = mean(f1) - f1$
5: $f2 = f2 - mean(f2)$
6: $f1 = ones * (f1 > beta)$
7: $f2 = ones * (f2 > beta)$
8: $f = f1 + f2$
9: $f = ones * (f > 0.)$

在算法 1中，我们对一张真实图像用Sobel算子提取得到其横向和纵向的边缘检测图，对两张边缘检测图进行最大值规约和最小值规约得到两张新的边缘检测融合图，然后两张边缘检测融合图分别与各自的平均像素值求差，再对两张差值图根据设定像素阈值进行二值化处理，两张二值图求和后再进行完全的二值化，最后得到的就是我们需要的结构特征图。 In Algorithm 1 we use Sobel operator to extract the horizontal and vertical edge detection maps from a real image, each perform reduce maximum and reduce minimum to obtain two edge detection fusion maps, each fusion map calculate the difference with average pixel value, the two difference maps are binarized according to the set pixel threshold, and the two binary images are

summed and then completely binarized. The final result is the structural feature map we need.

2.3 随机结构特征图的生成训练Training of Random Structural Feature Map Generation

在生成结构特征图时，(Shin et al. 2018)仍然需要真实的MRI作为输入来得到生成的结构特征图，这大大降低了生成数据的多样性，(Costa et al. 2017)实现了一种从多维正态分布生成视网膜血管分布图的方法，在其基础上，我们设计了一种从随机噪声生成脑部结构特征图的方法，无需额外数据且具有更好的多样性。具体来说，我们结合了变分自编码器与生成对抗网络的特点设计了一种混合网络。首先，我们从真实影像提取得到结构特征图，再通过VAE的编码器将其编码为一个均值矩阵和一个方差矩阵，再与一个随机正态分布矩阵融合为一个近似正态分布矩阵，通过损失约束其逐渐逼近标准正态分布。然后，我们再用VAE的解码器实现从该近似正态分布重建生成结构特征图。解码器通过结构特征图的自监督重建损失进行训练。对于近似正态分布矩阵的损失约束，我们没有采用VAE原本的编码器损失，而是通过一个编码分布鉴别器为编码器提供对抗性损失，此编码分布鉴别器以正态分布矩阵为正样本、输入解码器的近似正态分布矩阵为负样本进行学习。此外，我们还通过$L2$正则损失指导均值矩阵的均值逼近0值，标准差矩阵的均值逼近1值。同时，我们用另一个鉴别器对从真实MRI提取的结构特征图和随机生成的结构特征图进行鉴别学习，并为解码器提供对抗性损失，使得从随机正态分布解码生成的结构特征图越来越逼真。 When generating the structural feature map, (Shin et al. 2018) still needs to input the real modal image to get the generated structural feature map, which greatly reduces the diversity of generated data, and (Costa et al. 2017) implements a method for generating retinal blood vessel distribution maps from multidimensional normal distribution. On the basis of this, we design a method for generating brain structural feature maps from random
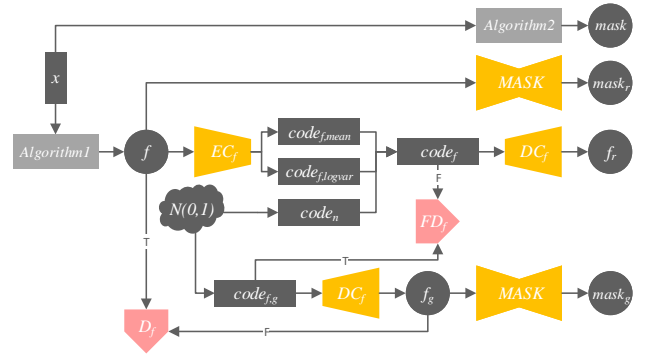

图 2: 随机结构特征图的生成训练.Training of Random Structural Feature Map Generation.

noise, which has better diversity and no additional data. Specifically, we design a hybrid network combining the characteristics of VAE and GAN. First, we encode the structural feature map extracted from real image into a mean matrix and a variance matrix through the VAE encoder, then fuse with a random normal distribution matrix to form an approximate normal distribution matrix, and gradually approach the standard normal distribution through the loss constraint. Then, we use VAE decoder to reconstruct the structural feature map from the approximate normal distribution matrix. The decoder is trained by self-supervised reconstruction loss of structural feature maps. For the constraint of approximate normal distribution matrix, we do not use the VAE encoder loss, but add a code distribution discriminator. The code distribution discriminator learns normal distribution matrix as a positive sample and latent feature matrix as a negative sample, and provides adversarial loss for encoder. Meanwhile, we use $L2$ regular loss to guide the mean matrix with a mean of 0 and the variance deviation matrix with a mean of 1. In addition, we use another discriminator to receive structural feature map extract from real MRI and randomly generated structural feature map for adversarial learning, so that the generated structural feature map becomes more and more realistic.

为了防止通过结构特征图生成的脑MRI像素区域超出结构特征图的脑轮廓线之外，我们还训练

了一个从脑结构特征图获取脑部区域掩膜的生成器$MASK$，该生成器与结构特征图的生成训练进行同步训练。训练时，将真实脑MRIx通过掩膜提取算法提取得到的掩膜作为训练标签数据，掩膜的提取算法如算法2所示。 In order to prevent the generated brain MRI pixel area from exceeding the brain outline of the structural feature map, we train a generator $MASK$ that acquires the brain area mask from the brain structure feature map. The generator is synchronized with the training of structural feature map generation. During training, the mask extracted by the real brain MRIx through the mask extraction algorithm (Algorithm 2) is used as label data.

Algorithm 2 Mask Extraction

1: Input a real image x, p is expanded pixel value
2: $mask = 1.0 - ones * (x > 0.)$
3: $shape = get\_shape(x)$
4: $mask = resize(mask, size = [shape[1] + p, shape[2] + p])$
5: $mask = crop\_padding(mask, crop\_length = p, crop\_width = p)$

　　如图2所示，从标准正态分布解码得到随机结构特征图的具体处理过程如下： As shown in Fig. 2, the specific processing procedure for decoding the random structure feature map from standard normal distribution is as follows:

- 从真实MRIx中用结构特征提取方法得到结构特征图f，用掩膜提取算法(算法 2)生成掩膜$mask$； The structural feature map f is obtained from real MRIx using the structural feature extraction method, and the mask $mask$ is obtained by the mask extraction algorithm(Algorithm 2);

- 用编码器EC_f对结构特征图f进行编码获得$code_{f,mean}$及$code_{f,logvar}$，从正态分布$\mathcal{N}(0,1^2)$的获取随机噪声$code_n$，由三个编码求得近似正态分布矩阵$code_f = code_{f,mean} + exp(0.5 * code_{f,logvar}) * code_n$； Encode f with encoder EC_f to get $code_{f,mean}$ and $code_{f,logvar}$,

get a random noise $code_n$ from multidimensional normal distribution $\mathcal{N}(0,1^2)$, the approximate normal distribution matrix is obtained from three codes $code_f = code_{f,mean} + exp(0.5 * code_{f,logvar}) * code_n$;

- 用解码器DC_f对$code_f$解码得到重建的结构特征图f_r； Decode $code_f$ with decoder DC_f to obtain the reconstructed structural feature map f_r;

- 用掩膜生成器$MASK$从f提取得到掩膜$mask_r$； Use mask generator $MASK$ to extract mask $mask_r$ from f;

- 随机生成符合正态分布$\mathcal{N}(0,1^2)$的矩阵$code_{f,g}$； Randomly generate a matrix $code_{f,g}$ that obeys normal distribution $\mathcal{N}(0,1^2)$;

- 用解码器DC_f对$code_{f,g}$解码得到生成的随机结构特征图f_g； Decode $code_{f,g}$ with decoder DC_f to get the generated random structure feature map f_g;

- 用掩膜生成器$MASK$对f_g提取得到掩膜$mask_g$； Use mask generator $MASK$ to extract mask $mask_g$ from f;

- 结构特征图鉴别器D_f分别对f和f_g进行鉴别，将前者鉴别为真，后者鉴别为假； Structural feature discriminator D_f identifies f and f_g respectively, identifying the former as true and the latter as false;

- 编码分布鉴别器FD_f分别对$code_f$和$code_{f,g}$进行鉴别，将前者鉴别为假，后者鉴别为真。 Code distribution discriminator FD_f discriminates between $code_f$ and $code_{f,g}$, respectively, identifying the former as false and the latter as true.

　　训练过程中的各项损失函数如下，其中，$\omega_{i,j}$为各损失项的权重： In training, we perform adversarial training through discriminator D_f to make the structural feature map decoded by decoder more realistic. In addition, the adversarial training is performed by the feature discriminator FD_f, so that encoder EC_f can encode structural feature map f to standard normal distribution.

The complete loss items are as follows, where $\omega_{i,j}$ is the weight of each loss item:

- **编码鉴别器损失Discriminator Loss of Code Distribution**

$$loss_{FD_f} = \|FD_f(code_{f,g}) - 1\|_2^2 + \|FD_f(code_f)\|_2^2$$

- **结构特征图鉴别器损失Discriminator Loss of Structural Feature Map**

$$loss_{D_f} = \|D_f(f) - 1\|_2^2 + \|D_f(f_g)\|_2^2$$

- **对抗性损失Adversarial Loss**

$$loss_{G_f} = \|FD_f(code_f) - 1\|_2^2 + \|D_f(f_g) - 1\|_2^2$$

- **结构特征编码的分布监督损失Supervised Loss of Structural Feature Code Distribution**

$$loss_{normal} = \|mean(code_{f,mean})\|_2^2 + \\ \|mean(exp(0.5 * code_{f,logvar})) - 1\|_2^2$$

其中，$mean()$函数为均值函数。 where $mean()$ is a mean function.

- **结构特征图及掩模的自监督损失Self-supervised Loss of Structural Feature Map and Mask**

$$loss_{sv} = \|f - f_r\|_2^2 + \|f_r * mask\|_2^2$$

- **掩膜生成器损失Mask Generator Loss**

$$loss_{mask} = \|mask - mask_r\|_2^2 + \|f * mask_r\|_2^2 + \\ \|f_r * mask_r\|_2^2 + \|f_g * mask_g\|_2^2$$

2.4 真实MRI重建和转换训练Real MRI reconstruction and translation training

我们在真实的MRI上进行MRI的重建和转换训练，用到了一套MRI编码器、MRI解码器和MRI鉴别器，以及一组病灶标签生成组件。这个训练过程中的全部组件会在后面的多模态MRI生成训练部分中介绍对它们进行的其他训练，并且本节的训练过程与多模态MRI生成训练是同步进行的。我们通过在
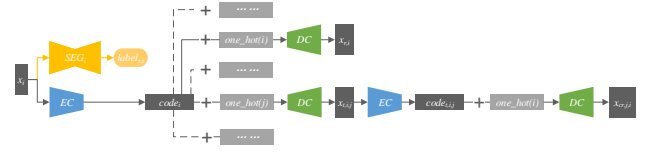

图 3: 辅助的模态重建和模态转换训练.Auxiliary modality reconstruction and modality translation training.

真实数据上的同步MRI重建和转换训练来约束各个组件在多模态MRI生成的过程中完成我们指定的任务。此外我们还通过一个编码鉴别器来对两个训练过程进行一致性指导。鉴别器训练过程如图 5所示。 We perform MRI reconstruction and translation training on real MRI, using a set of MRI encoder, MRI decoder and MRI discriminator, as well as a set of lesion label generation components. All of the components of this training process will be described in the subsequent multimodal MRI generation training section, and the training process in this section is synchronized with the multimodal MRI generation training. We constrain each component to complete our assigned tasks during multimodal MRI generation by synchronous MRI reconstruction and translation training on real data. In addition, we also use a code discriminator to guide the consistency of the two training processes. The discriminator training process is shown in Fig. 5

如图 3所示，MRI重建和转换时，编码器将模态i的真实MRIx_i编码得到语义特征图$code_i$，然后我们将其与不同的条件向量堆叠，通过解码器解码出全部的模态。循环重建时，我们对所得到的转换图采用编码器全部进行再编码，将全部再编码得到的语义特征图均与模态i的条件向量进行连接，最后再用解码器全部解码得到循环重建的$x_{rc,j,i}$。 MRI重建的循环重建都是自监督训练。在上述过程中，我们以原始输入模态x_i对应的病灶标签l_i作为病灶生成训练的监督标签，对x_i用病灶标签生成组件得到$l_{r,i}$。 As shown in Fig. 3, when the MRI is reconstructed and translated, the encoder encodes the real MRI x_i of modality i to obtain the semantic fea-

ture map $code_i$, then we connect it to different conditional vectors and decode all the modalities through the decoder. In cycle-reconstruction, we use encoder to re-encode all the obtained translation images, connect all the re-encoded semantic feature maps with the conditional vector of modality i, and finally decode them by decoder to get cycle-reconstruction image $x_{rc,j,i}$. 【 】 In the above process, we use the lesion label l_i of the original input modality x_i as supervised label for the lesion generation training, and use lesion label generation components for x_i to get $l_{r,i}$.

我们的鉴别器组件独立更新,其他组件通过一个优化器更新训练,损失项包括鉴别器提供的对抗性损失、MRI重建自监督损失、MRI循环重建自监督损失、MRI循环重建一致性损失、语义一致性损失、病灶生成监督损失。详细损失如下,其中$x_{r,i}$表示模态i重建得到的MRI,$x_{t,j,i}$指由模态j转换生成的模态i的MRI,$d_{t,j,i}$和$c_{t,j,i}$分别为鉴别器对$x_{t,j,i}$的真假鉴别和类别鉴别结果,$x_{cr,j,i}$表示模态i转换为模态j再转换回模态i的MRI;$code_i$表示编x_i编码器编码后得到的语义特征图,$code_{t,i,j}$表示x_i转换生成的模态j的MRI再经过编码器编码后得到的语义特征图;l_i表示x_i的真实病灶标签,$l_{r,i}$表示x_i经过病灶标签生成组件生成的病灶标签: Our discriminator components are updated independently, and other components are updated through an optimizer. The loss items include the adversarial loss and category guidance loss provided by discriminator, self-supervised loss of MRI reconstruction, self-supervised loss of MRI cycle-reconstruction, consistency loss of MRI cycle-reconstruction, semantic consistency loss, and supervised loss of lesion generation.

The detailed losses are as follows, where $x_{r,i}$ represents the MRI reconstruct from modality i, and $x_{t,j,i}$ refers to MRI of modality i translated by modality j. $d_{t,j,i}$ and $c_{t,j,i}$ are the true/false discrimination and category discrimination results of the discriminator for $x_{t,i,j}$, $x_{cr,j,i}$ represents MRI that translate from modality i to modality j then translate back to modality i; $code_i$ repre-

sents the semantic feature map obtained from x_i by encoder, $code_{t,i,j}$ represents the semantic feature map obtained from $x_{t,i,j}$ by encoder; l_i represents the real lesion label of x_i, $l_{r,i}$ represents the lesion label generated by lesion label generation components from x_i :

- 鉴别器损失discriminator loss

$$loss_{D,assist} = \sum_{j=0,j\neq i} \sum_{i=0} (\|d_{t,j,i}\|_2^2 + \|c_{t,j,i} - i\|_2^2)$$

- 对抗性损失和类别指导损失adversarial loss and category guidance loss

$$loss_{G,assist} = \sum_{j=0,j\neq i} \sum_{i=0} (\|d_{t,j,i} - 1\|_2^2 + \|c_{t,j,i} - i\|_2^2)$$

- **MRI重建自监督损失self-supervised loss of MRI reconstruction**

$$loss_{sv} = \sum_{i=0} (\|x_i - x_{r,i}\|_2^2)$$

- **MRI循环重建自监督损失self-supervised loss of MRI cycle-reconstruction**

$$loss_{cycle} = \sum_{j=0,j\neq i} \sum_{i=0} (\|x_i - x_{cr,j,i}\|_2^2)$$

- **MRI循环重建一致性损失consistency loss of MRI cycle-reconstruction**

$$loss_{cycle,consistency} =$$
$$\sum_{k=0,k\neq j,k\neq i} \sum_{j=0,j\neq i} \sum_{i=0} (\|x_{cr,j,i} - x_{cr,k,i}\|_2^2)$$

- 语义一致性损失semantic consistency loss

$$loss_{code,consistency} =$$
$$\sum_{j=0,j\neq i} \sum_{i=0} (\|code_i - code_{t,i,j}\|_2^2)$$

- 病灶生成监督损失supervised loss of lesion generation

$$loss_{sv,l} = \sum_{i=0} \|label_i - label_{r,i}\|_2^2$$

2.5 结构特征图与病灶分割标签的融合 Fusion of structural feature maps and lesion segmentation labels

结构特征图与病灶分割标签融合时，我们先从随机标准正态分布矩阵生成结构特征图f_g，再随机选择合适的病灶分割标签$label$，然后再将包含n个类别的病灶分割标签转为n个通道的独热矩阵$onehot_l$，每个通道对应一个分割类别，每个通道内的像素值为0或1，与对应类别分割位置相同的区域像素值为1其余部分为0，这样各个1像素区域与分割标签图中的各个分割区域就是配准的。接下来，我们将$onehot_l$的每个通道与f_g按位求取加权和，就得到一个新的融合了f_g和$label$信息的矩阵。 When the structural feature map is fused with the lesion segmentation label, we first generate structural feature map f_g from random standard normal distribution matrix, then randomly select the appropriate lesion segmentation label $label$, and then the lesion segmentation label containing n categories is converted into a one-hot matrix $onehot_l$ of n channels, and each channel corresponds to a segmentation category, the pixel value in each channel is 0 or 1. The pixel value of the same area as the corresponding category segmentation position is 1 and the rest is 0, so that each 1 pixel area is registered with each segmentation area in the segmentation label. Next, we calculate the weighted sum of each channel of $onehot_l$ with f_g, and get a new matrix that fuses the information of f_g and $label$.

如果结构特征图f'是从随机MRIx中提取的，那么提取出的结构特征有可能包含肿瘤结构信息，会对随机标签l中的肿瘤信息产生干扰而影响融合后生成的MRI，所以f'需要在与随机标签$label$融合前消除肿瘤信息，得到无肿瘤信息的结构特征图f，使生成图像的肿瘤信息只来源于标签$label$。我们对x的分割标签$label_x$通过算法2生成无边界扩充的分割掩膜$mask_{l,x}$,则$f = mask_{l,x} \times f'$。 If the structural feature map f' is extracted from the random MRI x, then the extracted structural features may contain tumor structure information, which may interfere with the tumor infor-
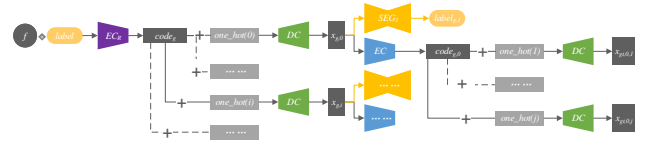

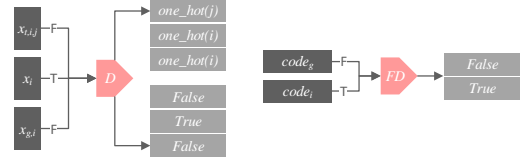图 4: 多模态MRI生成.generation of Multimodal MRI.

图 5: 真实MRI重建和转换训练和多模态MRI生成训练过程中的鉴别器训练. reconstruction and translation training of real MRI and discriminator training during multimodal MRI generation training.

mation in random label l and affect the fusion generation MRI, so f' needs to eliminate the tumor information before fusing with the random label $label$, and get the structural feature map f without tumor information, so that the tumor information of the generated image is only derived from the label $label$. We generate a mask without boundary expansion $mask_{l,x}$ for segmentation label $label_x$ of x by the Algorithm 2, then we have $f = mask_{l,x} \times f'$.

由于随机选择的病灶的位置上可能出现在结构特征图的脑部轮廓之外，因此我们选取标签图时需要用算法2获取结构特征图的脑部区域掩膜$mask$，若$mask$与选取的$label$求积后为0，则说明肿瘤标签像素在$mask$的脑轮廓内部，可以采用，否则需要重新选取$label$。 Since the location of the randomly selected lesion may appear outside the brain contour of structural feature map, we need to use the Algorithm 2 to obtain the brain region mask $mask$ of the structural feature map. If the product of $mask$ and the selected $label$ is 0, then the tumor label pixel is inside the brain contour of $mask$, which can be adopted, otherwise the $label$ needs to be re-selected.

2.6 多模态MRI生成训练Multimodal MRI generation training

我们通过算法 1从真实MRI提取结构特征图f,并随机选择真实的病灶标签$label$，通过前述结构特征图与病灶分割标签的方法进行融合。结构特征图与分割标签图的信息融合图包含了目标部位的基本解剖结构信息和病灶信息，从该图生成多模态图比直接从随机噪声生成多模态MRI更易训练，生成的MRI更加合理和逼真。多模态MRI生成过程如图4所示，首先，我们使用一个单独的融合图编码器对信息融合图进行编码得到语义特征图，语义特征图与不同的条件向量堆叠后通过一个MRI解码器解码，得到不同模态的合成图。我们通过一个MRI鉴别器提供的对抗性损失和类别指导损失来使得生成的各个模态的合成图逼近于真实的MRI。各个模态的合成图再通过一个MRI编码器得到语义特征图，然后这些语义特征图与不同的条件向量堆叠后通过MRI解码器解码就实现了模态的转换，我们通过损失对所有语义特征图和转换图进行一致性约束，以此保证了生成的多模态MRI的互相配准。此外，我们使用一组病灶标签生成组件从各合成MRI中分割还原出肿瘤病灶分割标签，确保生成的多模态影像根据输入病灶标签生成了对应的病灶内容。 We extract the structural feature map f from the real MRI by the Algorithm 1, and randomly select the real lesion label *label*, and merge with the lesion segmentation label by the above fusion method. The fusion map contains basic anatomical information and lesion information of the target site. The multimodal MRI generated from the fusion map is easier to train than the multimodal MRI generated directly from random noise, and the generated MRI is more reasonable and realistic. The multimodal MRI generation process is shown in Fig. 4. First, we use a fusion map encoder to encode fusion map to obtain the semantic feature map. The semantic feature map is stacked with different conditional vectors and decodes by MRI decoder to obtains synthesis image of different modalities. We use adversarial loss and category guidance loss provided by MRI discriminator to constrain synthesis im-

age to approximate real MRI. And images of each modalities are then encoded by MRI encoder to obtain semantic feature maps. These semantic feature maps are stacked with different conditional vectors and decoded by MRI decoder to realize the modal translation. We constrain the consistency of all semantic feature maps and translation images by loss, thus ensuring the mutual registration of generated multimodal MRI. In addition, we used a set of lesion label generation components to segment the tumor lesion segmentation labels from each synthetic MRI to ensure that the generated multimodal images have generated corresponding lesion content based on the input lesion label.

我们的鉴别器组件独立更新；病灶标签生成组件仅在前面章节中的真实MRI重建和转换训练中采用真实数据训练更新，在本节合成训练过程中病灶标签生成组件仅用于为MRI生成组件提供病灶生成指导损失；其他的组件通过一个优化器更新训练。多模态MRI生成过程的具体损失函数如下，其中d_i和c_i为鉴别器$D(x_i)$的真假鉴别输出和类别鉴别输出,$d_{g,i}$,$c_{g,i}$为$D(x_{g,i})$的输出；$x_{g,i}$为模态i的合成图，$x_{gt,j,i}$为模态j的合成图转换生成的模态i的转换图；$code_g$为输入信息编码后的语义特征图，$code_{g,i}$为x_i编码后的语义特征图；l为输入的标签图，$l_{g,i}$为$x_{g,i}$通过病灶标签生成组件得到的标签图；f为输入的结构特征图，$f_{g,i}$为从$x_{g,i}$通过算法 1提取得到的结构特征图：

- 鉴别器真假鉴别损失

$$loss_D = \sum_{i=0}(\|d_i - 1\|_2^2 + \|d_{g,i}\|_2^2)$$

- 鉴别器模态鉴别损失

$$loss_{D,class} = \sum_{i=0}(\|c_i - i\|_2^2 + \|c_{g,i} - i\|_2^2)$$

- 对抗性损失

$$loss_G = \sum_{i=0}(\|d_{g,i} - 1\|_2^2)$$

- 模态类别指导损失

$$loss_{G,class} = \sum_{i=0}(\|c_{g,i} - i\|_2^2)$$

- 输入的结构特征图的重建自监督损失

$$loss_{sv,f} = \sum_{i=0}(\|f - f_{g,i}\|_2^2)$$

- 病灶标签生成监督损失

$$loss_{sv,l} = \sum_{i=0}(\|label - label_{g,i}\|_2^2)$$

- MRI配准监督损失

$$loss_{trans} = \sum_{j=0,j\neq i}\sum_{i=0}(\|x_{g,i} - x_{gt,j,i}\|_2^2)$$

- 语义一致性损失

$$loss_{trans,code} = \|code_g - code_{g,i}\|_2^2 + \sum_{j=0,j\neq i}\sum_{i=0}(\|code_{g,i} - code_{g,j}\|_2^2)$$

2.7 病灶标签生成指导方案

我们设计了如下三种病灶标签生成组件来提供多模态MRI生成训练中病灶生成的指导损失：

- **单分割器方案** 每个模态由一个共同的完整的分割器从合成的MRI还原得到各自的病灶标签。

- **单病灶编码器+多病灶解码器方案** 每个模态由一个采用共同的病灶编码器与每个模态的独立的病灶解码器组合得到的分割器，从合成的MRI还原得到各自的病灶标签。

- **多分割器方案** 每个模态由一个独立的完整的分割器从合成的MRI还原得到各自的病灶标签。

上述三种方案的损失函数与前文所述损失函数一致，三种方案中的各个组件均只使用真实MRI重建和转换训练中的病灶生成监督损失进行训练。

2.8 构建合成数据集

如图所示，我们通过训练好的结构特征图解码器即可从随机生成的正太分布矩阵生成任意数量的结构特征图。然后，我们对原始的标签集进行了随机的缩放、旋转、平移、翻转等改变得到随机病灶标

图 6: 构建合成数据集.

签集。我们再将随机生成的结构特征图和从随机病灶标签集中随机选择的病灶标签融合，同样地，我们通过掩膜生成器$MASK$生成结构特征图的掩膜，可以筛选得到合适的随机病灶标签。最后，我们通过多模态MRI生成组件即可从融合信息图中生成配准的多模态MRI，选取的病灶标签就是生成的多模态MRI的病灶标签。由此，我们可以从随机正态分布矩阵构建带有病灶标签的多模态配准MRI数据集。

由于训练时去除肿瘤信息操作的影响，合成的结构特征图中，存在一些质量较差的脑轮廓未闭合结构特征图，我们对此设计了一个结构特征图过滤算法。首先，我们使用生成器生成一张结构特征图和其对应的掩膜，我们先对结构特征图进行高斯模糊(Wink and Roerdink 2004)，再采用OpenCV【】提供的轮廓查找算法和填充算法获取高斯模糊图所有的闭合轮廓并进行填充，这样我们得到一个采用传统算法的得到的掩膜，最后我们计算两张掩膜的均差(MAE)。若MAE低于我们设定的阈值则说明该结构特征图主要的脑部轮廓较为完整，该特征图可以使用；否则则说明该结构特征图主要的脑部轮廓有残缺，采用传统算法得到的掩膜内部是空心的，与生成器生成的掩膜差异较大，因此，需要重新生成。算法表示如下：

从筛选出来的结构特征图和匹配的病灶标签得到的多模态MRI中，同样存在病灶信息生成情况较差的样本。此时，我们通过预先训练好的病灶分割网络对我们的合成MRI数据进行分割，然后将分割结果与输入的病灶标签进行骰子评分评估，可以过滤得到评分高于设定阈值（默认0.95）的样本。

经过多重筛选，我们得到最终的由随机结构特征图、配对的掩膜、随机病灶分割标签、多模态MRI组成的合成数据集。我们要求经过分割过滤后的数据集使用在真实数据上训练得到的分割网络进行病灶分割时，得到的分割标签与数据集中的标签进行骰子分数评估能取得0.98以上的分数的数据

Algorithm 3 Structural feature map filtering

1: **function** $GetMaskFromF(img)$
2:     $contours = OpenCV.findContours(img)$
3:     $img = OpenCV.drawContours(img, contours)$
4:     **return** img
5: **end function**
6:
7: $mae = 0.05$
8: **do**
9:     $f, m = Generator()$
10:     $m' = GetMaskFromF(f)$
11: **while** $MAE(m', m) <= mae$

图 7: 病灶分割.

集才能用于数据可用性验证实验。

2.9　病灶分割训练

我们的病灶分割训练过程如图所示，为了验证合成数据中是否生成了与随机输入的病灶标签一致的病灶信息，我们用真实的数据为每个模态单独训练一个独立的病灶分割网络，并在真实数据集中进行分割能力测试。然后使用训练好的分割器对合成数据集中的影像进行分割，将分割结果与输入的病灶标签比对评估，以此检验合成的影像中包含了预期的病灶信息。此外，我们还采用由不同数据量的合成数据和真实数据构建的数据集来训练病灶分割网络，训练充分后再在真实测试数据集上进行分割能力测试，以验证合成数据的可用性。

分割训练的损失函数如下，其中$label_{r,i}$表示x_i经过病灶分割器生成的病灶标签：

$$loss_l = \sum_{i=0} \|label_i - label_{r,i}\|_2^2$$

3　实验

3.1　BRATS2015数据集

我们采用了公开的BRATS2015(Menze et al. 2014)数据集进行实验，该数据集包含已配准的T1、T2、T1c、Flair四个模态，训练集每个模态有274张3D MRI，大小为155×240×240，同时配有274张相同尺寸的肿瘤分割标签。我们将样本按9:1划分训练集和测试集，取每张3D MRI第55-105间的50个slice构建2D的数据集。在数据预处理阶段，我们将每张图进行了标准化。

3.2　BRATS合成数据集

我们采用 2.8中的方法构建了一个配准的包含T1、T2、T1c、Flair四个模态的具有肿瘤标签的合成数据集。合成数据集样本的尺寸与BRATS2015数据集一致，但样本的多少可以根据实验需要进行任意数量的合成。

3.3　BRATS增强数据集

我们对原始的BRATS2015数据集进行了随机的缩放、旋转、平移、翻转等改变，得到增强数据。增强数据集样本的尺寸与BRATS2015数据集一致，但样本的多少可以根据实验需要进行任意数量的生产。

3.4　训练设置

每项实验的迭代次数与BRATS2015训练数据集的100个epoch相等；基础学习率分别为1e-4，无权重衰减；采用优亚当优化器，beta1取0.5；在输入层进行0.1的Dropout；Batch size为1；在生成器中使用均值滤波器的参数进行参数初始化，具体来说，对于一个卷积核尺寸为$[k, k, f]$的卷积层，我们采用random normal initializer设定该层卷积核的$k \times k \times f$个参数均设置为$1/(k \times k \times f)$, 偏置量为 0；在鉴别器中我们使用0均值和标准差为0.2的random normal initializer，偏置量为0。我们采用骰子分数(Dice 1945)和均方差（MSE）(Prasad and Rao 1990)进行分割结果的评估，评估结果为2D图像的评估结果的均值，每项实验训练四次保留最佳结果。

3.5　病灶生成组件各方案对比实验

我们使用在处理后的BRATS2015数据集的训练集对病灶分割网络进行了相同迭代步数的充分训练，然后我们在BRATS2015数据集的测试集和采用不同

表 1: 病灶检测实验结果.

synthetic method	test data type	MSE	Dice Score
-	real	0.026	0.915
1SEG	synthetic	0.053	0.741
1ECL+4DCL	synthetic	0.055	0.808
4SEG	synthetic	0.043	0.838

表 2: 合成数据可用性验证实验结果.

序号	真实量	合成量	增强量	混合方式	MSE	Dice Score
1	15070	0	0	无混合	0.026	0.915
31	15070× 0.5	0	0	无混合	0.032	0.902
2	0	15070	0	无混合	0.205	0.708
3	0	15070× 2	0	随机混合	0.206	0.736
4	0	15070× 3	0	随机混合	0.205	0.754
7	15070× 0.1	15070	0	先假后真	0.031	0.908
8	15070× 0.1	15070× 2	0	先假后真	0.028	0.907
9	15070× 0.1	15070× 3	0	先假后真	0.030	0.907
13	15070× 0.2	15070× 0.8	0	随机混合	0.041	0.850
12	15070× 0.5	15070× 0.5	0	随机混合	0.031	0.904
14	15070× 0.8	15070× 0.2	0	随机混合	0.024	0.935
32	15070	15070× 0.2	0	随机混合	0.025	0.921
33	15070	15070× 0.5	0	随机混合	0.023	0.939
34	15070	15070× 0.8	0	随机混合	0.026	0.916
15	15070	15070	0	随机混合	0.027	0.913
18	15070	15070× 2	0	随机混合	0.033	0.901
19	15070	15070× 3	0	随机混合	0.034	0.897
35	15070	0	15070× 0.2	随机混合	0.027	0.911
36	15070	0	15070× 0.5	随机混合	0.025	0.927
37	15070	0	15070× 0.8	随机混合	0.026	0.920
22	15070	0	15070	随机混合	0.026	0.915
23	15070	0	15070× 2	随机混合	0.032	0.898
24	15070	0	15070× 3	随机混合	0.036	0.885
16	15070	15070	0	先真后假	0.195	0.795
17	15070	15070	0	先假后真	0.021	0.940

病灶生成组件方案的未经分割器筛选的的BRATS合成数据集上分别进行分割测试，除了测试数据来源的不同外，测试数据的样本量等其他条件完全相同。其中，我们在真实数据上采用的分割方案为章节2.7中的多分割器方案，即每个模态各训练一个独立的分割器。

3.6 合成数据可用性验证实验

如表所示，我们将真实的BRATS2015训练数据与BRATS合成数据进行了不同数量的混合，再用构建的混合数据集进行分割训练，最后再在真实的BRATS2015测试数据上进行模型的分割能力评估，所有实验都进行训练相同迭代步数的充分训练，除了训练数据源的不同外其他条件完全相同。同时，我们还进行了单独的合成数据的训练、真实数据与通常的数据增强数据的混合训练作为对比。我们设定了随机混合、先真后假、先假后真三种数据混合方式。我们选用实验 3.5中，在合成数据集上表现最好的分割方案来作为验证实验的分割方案。

4 结果

4.1 实验量化结果

病灶检测实验结果 如表 1所示，我们在BRATS2015训练数据经过相同的迭代步数的充分训练后，在真实的测试数据集上，分割测试结果达到了0.026的MSE和0.915的Dice Score。之后我们使用这个表现优秀的分割网络对我们未经过滤的合成数据进行分割测试，在与真实测试数据集相同数据量的合成数据集上，不同病灶标签生成组件设计方案都取得了较好的分割结果，其中每个模态训练一个独立的分割器的方案取得了最好的结果，Dice Score也达到了0.838。

合成数据可用性验证实验结果 如表 2所示，我们在不同的成分和数量的数据集上都经过训练后再在真实测试集上评估，得到了表中的结果。实验1在BRATS2015训练数据经过100个epoch的充分训练后，在真实的测试数据集上，分割测试结果达到了0.026的MSE和0.915的Dice Score。从表中实验2-4单独使用合成数据训练的结果看，合成数据与真实数据的训练结果仍然有一定差距，这说明合成数据不能完全替代真实数据充当训练集。实验7-9结果表明使用大量合成数据进行预训练，再在少量真实数据上微调能达到和实验1全使用真实数据训练十分接近的结果。这说明合成数据作为预训练数据集非常合适。实验12-14中一定比例的真实数据与合成数据随机混合，比例不同取得的结果差异很大，当两者比例相近时分割结果与实验1相差不大，合成数据比例偏高时，结果比实验1低，合成数据比例偏低时，能提供模型的泛化能力，取得高于实验1的结果。实验32-34，15,18-19中进一步尝试在全量的真实数据中添加不同数据量的合成数据，我们发现较少的合成数据能提高模型的泛化能力，起到数据增强的作用，合成数据越多增强效果越好，但当合成数据到

达一定比例后再继续增加将取得反效果，此时合成数据越多越使得真实数据的影响力下降。实验35-37和实验22-24中，我们使用通常的数据增强方法产生的增强数据来与前述合成数据的增强效果进行对比，我们发现在增强数据量与增强效果的变化趋势上，两者是一致的，但两者在具体的增强效果随着增强数据量变化的变化曲线上是有一些差异的。整体来说，在模型对增强数据量的敏感程度上，增强数据更加鲁棒，但合成数据能取得的增强效果的上限比曾强数据要高很多。在实验16-17中，我们对比实验15，发现与真实数据相同数量的合成数据，作为预训练数据先于真实数据训练时表现最好，作为增强数据与真实数据混合训练时效果居中，作为补充训练数据集在真实数据集之后训练则表现很差。

总的来说，我们发现当真实数据量较多时，可以使用少量的合成数据作为增强数据混合使用，也可以使用大量的合成数据先进行预训练，再在真实数据集上训练；当真实数据较少时，可以使用大量的合成数据进行预训练，再在少量真实数据上微调，最后能得到和完全真实数据训练相竞争的结果，这点我们与(Shin et al. 2018)的结论一致；我们不建议完全使用合成数据进行训练，与(Shin et al. 2018)的结论不同的是我们也不建议使用合成数据进行补充训练。

4.2 合成图像展示

图8展示了我们从随即正态分布矩阵生成的结构特征图示例。图9中展示了我们从随即正态分布矩阵生成的结构特征图、从结构特征图生成的对应的掩膜、随机选择的病灶分割标签、从结构特征图生成和的病灶分割标签生成的多模态MRI的几个示例。

5 结论与未来工作

我们基于条件生成对抗网络，通过无监督的训练，实现了能在已有单模态数据时可扩展出多模态影像数据并保留原模态的病灶信息，同时可从随机噪声生成配准的多模态医学影像并可自由添加病灶信息。我们通过病灶分割实验验证了合成的医学影像可以作为医学影像智能处理任务的预训练数据或
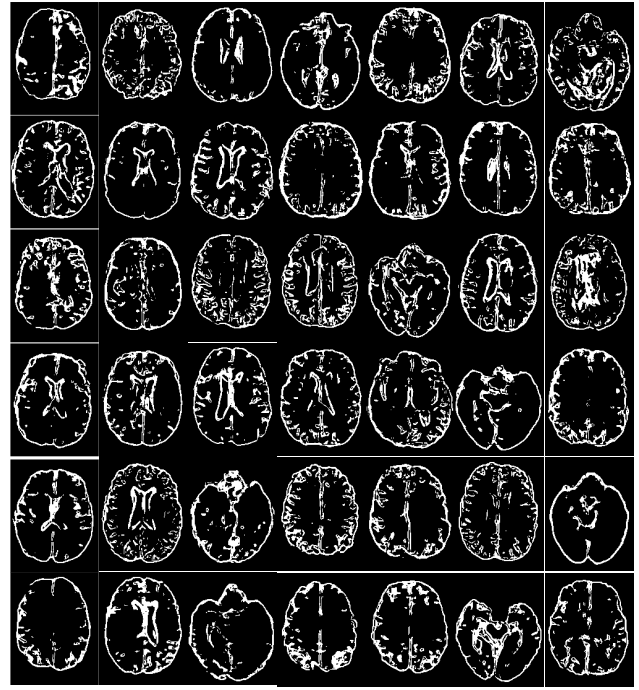

图 8: 合成的结构特征图.

增强数据来提高模型的泛化能力。具体来说，我们的贡献包括以下几点：

- 结构特征图提取方法。我们从医学影像直接提取解剖结构信息，无须训练，无需额外数据；

- 随机结构特征图生成方法。我们实现了从多维正态分布采样生成结构特征图，使结构特征图能便捷地大量生成并使最后合成的影像具有良好的多样性；

- 模态转换方法。我们实现了多模态脑MRI之间的互转，使单模态数据可转换生成多模态影像数据并保留原模态的病灶信息；

- 基于结构特征图生成多模态图方法。我们从真实影像提取的结构特征图及随机选择的标签生成带病灶标签的配准的多模态影像；

- 构建带标签的多模态配准数据集方法。我们组合使用随机结构特征图生成方法和基于结构特征图生成多模态图方法，实现了从多维正态分布随机生成结构特征图，结合随机选择的标签生成带标签的配准的多模态MRI数据；
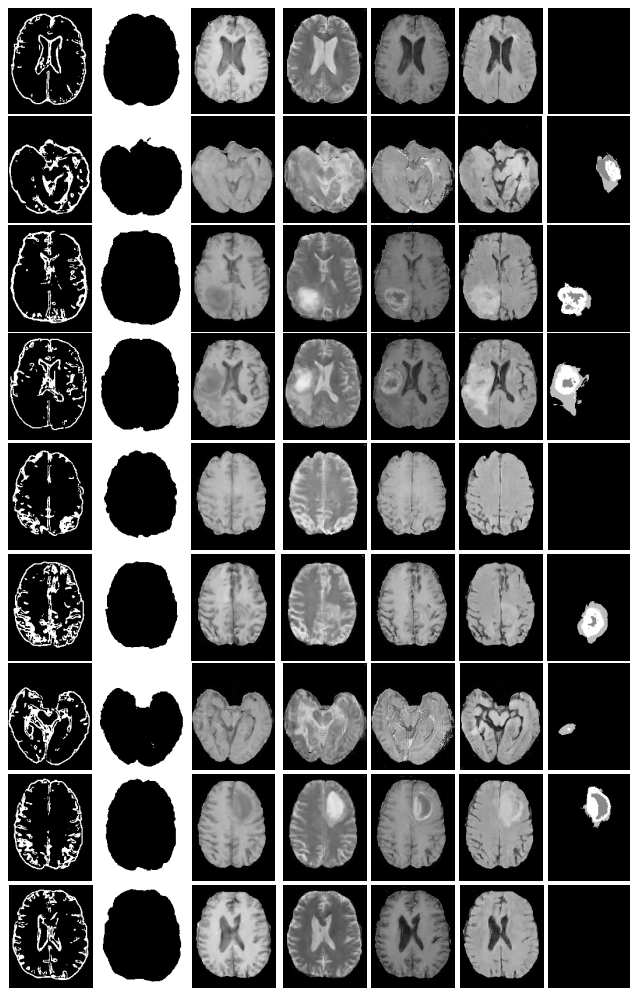
图 9: 从随机结构特征图和病灶标签生成多模态MRI.

- 合成数据可用性测试方法。我们将合成数据与真实数据数据集进行不同比重的混合，通过病灶分割网络验证了合成数据在分割训练中的提升效果。

未来，我们将进一步在CT、PET等不同模态和其他部位中对我们的方法进行改进，并将进一步简化训练过程和提升合成质量。

6   Acknowledgments

References

Burgos, N.; Cardoso, M. J.; Guerreiro, F.; Veiga, C.; Modat, M.; Mcclelland, J.; Knopf, A.; Punwani, S.; Atkinson, D.; Arridge, S. R.; et al. 2015. Robust ct synthesis for radiotherapy planning: Application to the head and neck region. *medical image computing and computer assisted intervention* 476–484.

Chartsias, A.; Joyce, T.; Giuffrida, M. V.; and Tsaftaris, S. A. 2018. Multimodal mr synthesis via modality-invariant latent representation. *IEEE Transactions on Medical Imaging* 37(3):803–814.

Choi, Y.; Choi, M.; Kim, M.; Ha, J.; Kim, S.; and Choo, J. 2018. Stargan: Unified generative adversarial networks for multi-domain image-to-image translation. *computer vision and pattern recognition* 8789–8797.

Costa, P.; Galdran, A.; Meyer, M. I.; Abramoff, M. D.; Niemeijer, M.; Mendonca, A. M.; and Campilho, A. 2017. Towards adversarial retinal image synthesis. *arXiv: Computer Vision and Pattern Recognition*.

Dice, L. R. 1945. Measures of the amount of ecologic association between species. *Ecology* 26(3):297–302.

G, R. L. 1965. Machine perception of three-dimensional solids. *Optical and Electro-Optical Infomation Processing*.

Goodfellow, I. J.; Pougetabadie, J.; Mirza, M.; Xu, B.; Wardefarley, D.; Ozair, S.; Courville, A. C.; and Bengio,

Y. 2014. Generative adversarial nets. *neural information processing systems* 2672–2680.

Huang, Y.; Shao, L.; and Frangi, A. F. 2017. Simultaneous super-resolution and cross-modality synthesis of 3d medical images using weakly-supervised joint convolutional sparse coding. *computer vision and pattern recognition* 5787–5796.

Isola, P.; Zhu, J.; Zhou, T.; and Efros, A. A. 2017. Image-to-image translation with conditional adversarial networks. *computer vision and pattern recognition* 5967–5976.

Joyce, T.; Chartsias, A.; and Tsaftaris, S. A. 2017. Robust multi-modal mr image synthesis. *medical image computing and computer assisted intervention* 347–355.

Kamnitsas, K.; Baumgartner, C. F.; Ledig, C.; Newcombe, V.; Simpson, J. P.; Kane, A. D.; Menon, D. K.; Nori, A. V.; Criminisi, A.; Rueckert, D.; et al. 2017. Unsupervised domain adaptation in brain lesion segmentation with adversarial networks. *information processing in medical imaging* 597–609.

Kingma, D. P., and Welling, M. 2014. Auto-encoding variational bayes. *international conference on learning representations*.

Krizhevsky, A.; Sutskever, I.; and Hinton, G. E. 2012. Imagenet classification with deep convolutional neural networks. *neural information processing systems* 141(5):1097–1105.

Liang, X.; Zhang, H.; Lin, L.; and Xing, E. P. 2018. Generative semantic manipulation with mask-contrasting gan. *european conference on computer vision* 574–590.

Menze, B.; Jakab, A.; Bauer, S.; Kalpathy-Cramer, J.; Farahani, K.; Kirby, J.; Burren, Y.; Porz, N.; Slotboom, J.; Wiest, R.; Lanczi, L.; Gerstner, E.; Weber, M.-A.; Arbel, T.; Avants, B.; Ayache, N.; Buendia, P.; Collins, L.; Cordier, N.; Corso, J.; Criminisi, A.; Das, T.; Delingette, H.; Demiralp, C.; Durst, C.; Dojat, M.; Doyle, S.; Festa, J.; Forbes, F.; Geremia, E.; Glocker, B.; Golland, P.; Guo, X.; Hamamci, A.; Iftekharuddin, K.; Jena, R.; John, N.; Konukoglu, E.; Lashkari, D.; Antonio Mariz, J.; Meier, R.; Pereira, S.; Precup, D.; Price, S. J.; Riklin-Raviv, T.; Reza, S.; Ryan, M.; Schwartz, L.; Shin, H.-C.; Shotton, J.; Silva, C.; Sousa, N.; Subbanna, N.; Szekely, G.; Taylor, T.; Thomas, O.; Tustison, N.; Unal, G.; Vasseur, F.; Wintermark, M.; Hye Ye, D.; Zhao, L.; Zhao, B.; Zikic, D.; Prastawa, M.; Reyes, M.; and Van Leemput, K. 2014. The Multimodal Brain Tumor Image Segmentation Benchmark (BRATS). *IEEE Transactions on Medical Imaging* 33.

Miao, S.; Piat, S.; Fischer, P. W.; Tuysuzoglu, A.; Mewes, P.; Mansi, T.; and Liao, R. 2018. Dilated fcn for multi-agent 2d/3d medical image registration. *national conference on artificial intelligence* 4694–4701.

Mirza, M., and Osindero, S. 2014. Conditional generative adversarial nets. *Computer Science* 2672–2680.

Nie, D.; Trullo, R.; Lian, J.; Petitjean, C.; Ruan, S.; Wang, Q.; and Shen, D. 2017. Medical image synthesis with context-aware generative adversarial networks. *medical image computing and computer assisted intervention* 417–425.

Osokin, A.; Chessel, A.; Salas, R. E. C.; and Vaggi, F. 2017. Gans for biological image synthesis. *international conference on computer vision* 2252–2261.

Prasad, N. G. N., and Rao, J. N. K. 1990. The estimation of the mean squared error of small-area estimators. *Journal of the American Statistical Association* 85(409):163–171.

Prewitt, J. 1970. Object enhancement and extraction. *Picture processing and Psychopictorics*.

Rezende, D. J.; Mohamed, S.; and Wierstra, D. 2014. Stochastic backpropagation and approximate inference in deep generative models. *international conference on learning representations* 1278–1286.

Shin, H.; Tenenholtz, N. A.; Rogers, J. K.; Schwarz, C. G.; Senjem, M. L.; Gunter, J. L.; Andriole, K. P.; and

Michalski, M. 2018. Medical image synthesis for data augmentation and anonymization using generative adversarial networks. *arXiv: Computer Vision and Pattern Recognition* 1–11.

Sobel, I. 1970. Camera models and machine perception. *Ph.D.dissertation*.

Van Nguyen, H.; Zhou, K. S.; and Vemulapalli, R. 2015. Cross-domain synthesis of medical images using efficient location-sensitive deep network. *medical image computing and computer assisted intervention* 677–684.

Vemulapalli, R.; Van Nguyen, H.; and Zhou, S. K. 2015. Unsupervised cross-modal synthesis of subject-specific scans. *international conference on computer vision* 630–638.

Wang, Z.; Bovik, A. C.; Sheikh, H. R.; and Simoncelli, E. P. 2004. Image quality assessment: from error visibility to structural similarity. *IEEE Transactions on Image Processing* 13(4):600–612.

Wink, A. M., and Roerdink, J. B. T. M. 2004. Denoising functional mr images: a comparison of wavelet denoising and gaussian smoothing. *IEEE Transactions on Medical Imaging* 23(3):374–387.

Zhang, Z.; Yang, L.; and Zheng, Y. 2018. Translating and segmenting multimodal medical volumes with cycle- and shape-consistency generative adversarial network. *computer vision and pattern recognition* 9242–9251.

Zhao, B.; Chang, B.; Jie, Z.; and Sigal, L. 2018. Modular generative adversarial networks. *european conference on computer vision* 157–173.

Zhu, J.; Park, T.; Isola, P.; and Efros, A. A. 2017. Unpaired image-to-image translation using cycle-consistent adversarial networks. *international conference on computer vision* 2242–2251.